Int. J. Therm. Sci. (2001) 40, 409–424

S1290-0729(01)01223-6/FLA

Gas–Diesel (dual-fuel) modeling in diesel engine environment

Cheikh Mansour [a], Abdelhamid Bounif [a*], Abdelkader Aris [a], Françoise Gaillard [b]

[a] *Université des Sciences et de la Technologie BP 1505, Elmnaouar, Oran, 31000 Algeria*

[b] *Centre National de la Recherche Scientifique, 1C Avenue de la Recherche Scientifique, 45071 Orléans cedex 2, France*

(Received 2 December 1999, accepted 7 July 2000)

Abstract — The aim of this paper is to investigate the emission and performance characteristics of a commercial diesel engine (Deutz FL8 413F) being operated on natural gas with pilot diesel ignition. A computer program has been developed to model the experimental data using a chemical kinetic reaction mechanism of the Gas–Diesel (dual-fuel) combustion. A detailed chemical kinetic reaction mechanisms of natural gas and NO_x were used to predict the main combustion characteristics (temperature, pressure and species concentrations) under the conditions of this study. The following sections include a description of the experimental facilities, discussion of numerical simulation and engine test results. The performance in terms of accuracy of the networks is assessed by comparison with the experiments. A reasonably good prediction of performance and emission was obtained by computation covering the whole range of the engine operating conditions. It can be summarized that the results of this study are satisfactory. © 2001 Éditions scientifiques et médicales Elsevier SAS

dual-fuel / natural gas / diesel engine / combustion / modeling / pollution

Nomenclature

A, B	Wiebe model constants	
A, b	Arrhenius law coefficients	
C	production rate of species	
C_s	specific consumption	$kg{\cdot}kW^{-1}{\cdot}h^{-1}$
C_p	mass-weighted specific heat	$J{\cdot}kg^{-1}{\cdot}K^{1}$
E	activation energy	$J{\cdot}mol^{-1}$
F	equivalence ratio	
h	specific enthalpy	$J{\cdot}kg^{-1}$
N	engine speed	rpm
$\dot{m}$	mass flow rate	$kg{\cdot}s^{-1}$
P	pressure	Pa
P_s	specific power	$kW{\cdot}L^{-1}$
Q	cylinder heat loss	$J{\cdot}s^{-1}$
T	temperature	K
t	time	s
u	specific internal energy	$J{\cdot}kg^{-1}$
V	instantaneous cylinder volume	m^3
W	molecular weight	$kg{\cdot}mol^{-1}$
X_b	fuel burning rate	
Y	species mass fraction	
$\Delta\varphi$	engine crank angle step	
Δt	time step	s
τ	ignition time	s
α, β, ν	stoichiometric coefficients	
ρ	mass density	$kg{\cdot}m^{-3}$
$\dot{\omega}_k$	molar production rate	$mol{\cdot}s^{-1}$

Subscripts

k	kth species
c	mean value during compression phase
a	inlet air

* Correspondence and reprints.

E-mail addresses: mansour@mail.univ-usto.dz (C. Mansour), bounif@mail.univ-usto.dz (A. Bounif), arisaek@yahoo.com (A. Aris), gaillard@cnrs-orleans.fr (F. Gaillard).

1. INTRODUCTION AND BACKGROUND

The Environmental Protection Agency (EPA) will place severe limits in exhaust emissions of heavy-duty diesel engines for urban bus and highway truck applications [1]. These regulations (*table I*) demand considerable advances in technology to be made by heavy-duty diesel engine manufacturers to ensure that their products

TABLE I
United States EPA Clean Air Act Amendments [1].

Urban bus heavy-duty engine emission standards in $g \cdot kW^{-1} \cdot h^{-1}$ measured during EPA heavy-duty engine test					Heavy-duty truck engine emission standards in $g \cdot kW^{-1} \cdot h^{-1}$ measured during EPA heavy-duty engine test				
Model year	NO_x	HC	CO	PM	Model year	NO_x	HC	CO	PM
1990	8.0	1.7	20.7	0.804	1990	8.0	1.7	20.7	0.800
1991	6.7	1.7	20.7	0.335	1991	6.7	1.7	20.7	0.330
1993	6.7	1.7	20.7	0.134	1994	6.7	1.7	20.7	0.013
1994	6.7	1.7	20.7	0.070	1998	5.3	1.7	20.7	0.013
1998	5.4	1.7	20.7	0.067					

will meet these regulations. There are several strategies that may be employed to reduce emissions including further refinement of treatment, particulate traps, and alternative fuels. Compressed natural gas (CNG) is an attractive alternative fuel for the urban bus market due to the availability of space for tank placement and centralized refueling infrastructure. In Algeria, the use of alternative fuels in particular natural gas has been identified as a potential choice for engine design. The seven overall research objectives are:

- identify the operating characteristics of CNG-fueled conversions;
- determine the environmental effects of CNG conversions;
- determine the cost effectiveness of using CNG as an alternative fuel in city vehicles;
- identify maintenance concerns;
- examine infrastructure support;
- recommend "go or no go" decisions of conversion by vehicle class type;
- disseminate project information of documented research.

Numerous works have been published over the last 15 years (Karim [2], Al-himyari et al. [3], Quader [4], Tasarek [5], Xianhua et al. [6], Boisvert et al. [7], Martin et al. [8], Mills [9], Acker et al. [10], Kingston et al. [11], Saturo et al. [12], Fraser et al. [13], Edwards et al. [14], Doughty et al. [15] and Blizzard et al. [16], Bounif et al. [17, 18]) where complex behaviors have been revealed and many underlying combustion mechanisms which are not well understood in the application of natural gas fueling to a diesel-type operating with a lean burn concept. The understanding and modeling of turbulent combustion in dual-fuel engines based on the combustion of liquid and gaseous fuel is still a difficult and challenging problem. Major difficulties generally arise from strong coupling between turbulent and molecular transport phenomena and chemical kinetics as well as from complex geometry of engine chambers. The practical importance attached to conception and optimization of these systems in order to achieve higher performances while decreasing the pollutant emission level. However, the interaction between fluid-turbulence and premixed or diffusion flames is particularly difficult to study experimentally. Analytical theories for turbulent flames with complex chemistry encounter even higher difficulties, especially when the characteristic times scales of fluid-turbulence and chemical reaction are the same order of magnitude. The turbulent combustion progresses simultaneously under different regimes: wrinkled flame, thickened flame, distributed combustion and auto-ignition. The auto-ignition of diesel fuel (DF) and natural gas (NG) following release inside a turbulent oxidant of elevated temperature is configuration relevant to diesel engine combustion [13] but detailed understanding of the time and spatial location of, and the subsequent flame development from, auto-ignition sites is still lacking [2].

The performance of natural gas engines has been investigated with promising results. The emissions aspects are less well investigated (Tesarek [5], Boisvert et al. [7], Mills [9], Saturo et al. [12] and Doughty et al. [15]) but preliminary results from testing are encouraging for the particulate matter (PM) and NO_x emission levels.

The objective of this work was to investigate the emission and performance characteristics of a commercial diesel engine (Deutz FL8 413F) being operated on natural gas with pilot diesel ignition. The diesel engine was converted to operate in a natural gas with diesel pilot ignition mode and was evaluated for performance and emission characteristics for both diesel and natural gas operation. Furthermore, a numerical simulation of the Gas–Diesel (dual-fuel) engine has been carried out with a modified Perfect stirred Reactor (PSR) Chemkins' code [17–20]). During the combustion phase, the range of pressure and temperature experienced by the reactants drawn into the engine

cylinder is particularly wide, all variables are continually changing in time, and consequently, the simulation was non-trivial. The fuel conversion rates of natural gas–diesel fuel oxidation in all the experimental engine conditions are determined from a simulation study which takes into account a detailed kinetic model previously established by Tan et al. [21–23] and Dagaut et al. [24] for natural gas and the Hautmann [25] model for Diesel fuel. The following sections of this paper include a description of the experimental facilities, discussion of numerical simulation and engine test results.

2. AVAILABLE TECHNOLOGIES AND DUAL-FUEL CONCEPT

Reciprocating internal combustion engines are generally divided in two categories, compression-ignition (CI) and spark-ignition (SI) engines:

- In CI engines (diesel engines), air is compressed at pressures and temperatures at which an easily ignitable fuel fires spontaneously when injected and burns progressively after ignition.
- Whereas, SI engines (Otto engines) running according to the Beau de Rochas cycle, the carburated mixture of air are and gaseous or gasified fuel which does not fire easily (high octane index), is compressed under its ignition point, then fired at a chosen instant, by an independent means.

In dual-fuel engines both types of combustion coexist together, a carburated mixture of air and high octane index gaseous fuel (natural gas) is compressed and then fired by a small liquid fuel injection which ignites spontaneously at the end of compression phase. The advantage of this type of engine resides in the fact that it uses the difference of flammability of two fuels. In case of lack of gaseous fuel, it is possible to run according to the diesel cycle; switching being possible when running and without load variation. The disadvantage is the necessity to have liquid diesel fuel available. Theoretically, the liquid fuel quantity necessary to fire is tiny (less than 1 %), but, it is not possible to inject with the given pump and injectors assemblies fuel quantities varying from 1 to 100 %. If we do not want the material to be doubled, we must be satisfied by injection of the minimum possible quantity of standard diesel fuel.

3. EXPERIMENTAL PERFORMANCE

The engine used in this study is a naturally aspirated, V-8 Deutz FL8 413F four cycle diesel engine. The basic engine characteristics of the test engine are summarized in *table II*. *Tables III* and *IV* include information on natural gas composition and the test fuel properties.

TABLE II
Test engine specifications.

Engine (four-cycle)	Diesel FL8 413F
Cylinders	8
Combustion system	Direct injection
Maximum engine speed at full load	2 500 rpm
Rated brake power	170 kW
Maximum brake torque at 1 500 rpm	735 Nm
Bore × stroke	125 × 130 mm
Compression ratio	18 : 1
Displacement	12 761 cc

TABLE III
Averaged composition of natural gas [59].

Composition	Mass %
Nitrogen N_2	6.26
Carbon dioxide CO_2	0.19
Ethane C_2	7.38
Propane C_3	2.108
Iso-butane iC_4	0.34
n-butane nC_4	0.53
Iso-pentane iC_5	0.09
n-pentane nC_5	0.1
C_{6+}	0.002
Helium He	0.18
Methane CH_4	82.82

TABLE IV
Test fuel properties.

Natural gas (NG)	
Density at 1 atm and 15 °C	0.73727 kg·m^{-3}
Compressibility factor	0.99785
Specific gravity (air = 1)	0.5910
Lower heating value	
by volume	36.20 MJ·m^{-3}
by mass	49.10 MJ·kg^{-1}
Mean molecular weight	17.423
Stoichiometric air–fuel ratio	15.894
Hydrogen carbon ratio	3.87
Diesel fuel (DF)	
Lower heating value	45.2 MJ·kg^{-1}
Density	836 kg·m^{-3}
Cetane number	62.2

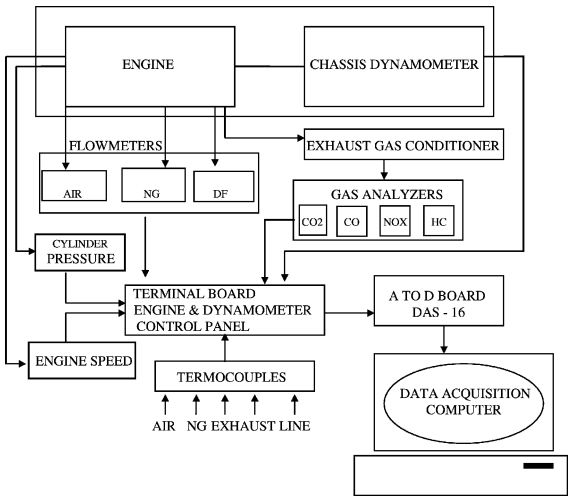

Figure 1. Synopsis of the experimental set-up.

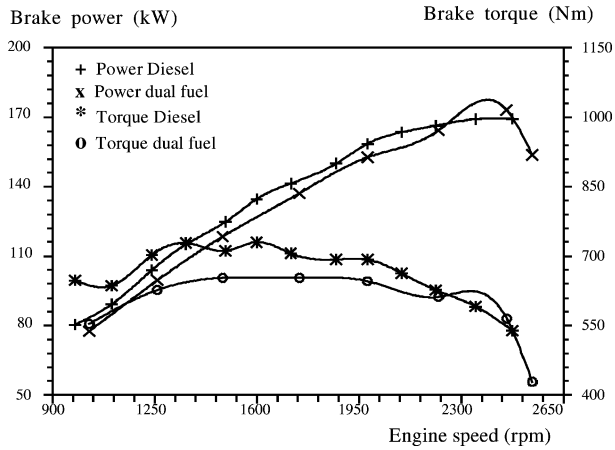

Figure 2. Brake power and brake torque as a function of engine speed for full load.

The dual-fuel mode uses compressed natural gas (CNG) as the primary fuel and small quantities of diesel pilot-fuel for ignition. The bus is equipped with a dual-fuel (combined use of diesel and CNG) DELTEC conversion kit. The kit allowed for engine operation on either 100 % diesel fuel or in a dual-fuel mode. In either case, the engine started and idled on diesel mode. Thus, engine starting and idling characteristics were identical to unmodified engine. In the dual-fuel mode, natural gas is introduced into the intake system, triggered by engine speed. Timing and duration of the pilot injection is performed by an electronically controlled hydraulic DELTEC system. The ratio of diesel pilot to natural gas is controlled by a metering valve, with diesel ratio (ratio of calorific value of diesel fuel to total calorific of fuels entering the combustion chamber) is kept approximately constant over the entire load range with a fixed metering valve position and CNG pressure. The natural gas was introduced into the intake air stream. Gas flow is measured by a fine wire anemometer and controlled using a manual, variable area and fine control needle valve. Engine intake air was filtered and measured with a laminar flow-meter. Diesel fuel flow rate is measured by two volumetric flow-meters, connected to the inlet manifold of the injection pump and to the outlet manifold. The flow-meters are connected by two photodiode cells to a data acquisition system.

The NUOVO-PIGNONE LPS 2000 chassis dynamometer engine test (*figure 1*) was equipped with a digital readout of engine speed, torque and power. A strain gage amplifier was placed in parallel to the dynamometer strain gage and a frequency-to-voltage convector was placed in series with the magnetic pick-up of the engine speed on the dynamometer. These modifications allowed engine speed and torque to appear on the dynamometer digital readout and to be simultaneously recorded by the computer data acquisition system. Therefore, two types of tests were performed in each measuring session, where the emission and performance levels were measured on a chassis dynamometer under steady and unsteady conditions. The compression ratio has been kept unchanged for the two versions engine test. *Figure 2* represents the evolution of full load brake power and brake torque in function of the engine speed under unsteady conditions. This corresponds to some phases of acceleration or of deceleration which the periods varies in mean from 1 to 10 s. Tests have been performed according to the DIN 70020 engine test Standard Norms. One observes a light power and torque losses in dual fuel version with regard to the diesel one, except around the speed of 2 400 rpm when the regulating system stops the fuel injection pump. This difference could be explained by the system response time of natural gas injection in the admission collector. When the engine speed rises up to 2 450 rpm, the brake torque and the brake power in dual-fuel version are slightly higher than in the diesel mode. *Figure 3* shows the evolution of the specific power and consumption versus engine speed for full load. One notices that at low engine speed the difference is important between the two versions (loss of power and higher consumption), but in high regimes the gap becomes less important. The evaluation of the specific consumption was based on the experimental results of the brake power and the consumption results under steady conditions. It was taken to be equal to brake power divided by the total injected volume (pilot diesel + natural gas volume in equivalent energetic). Because fuel heating values are different for diesel fuel

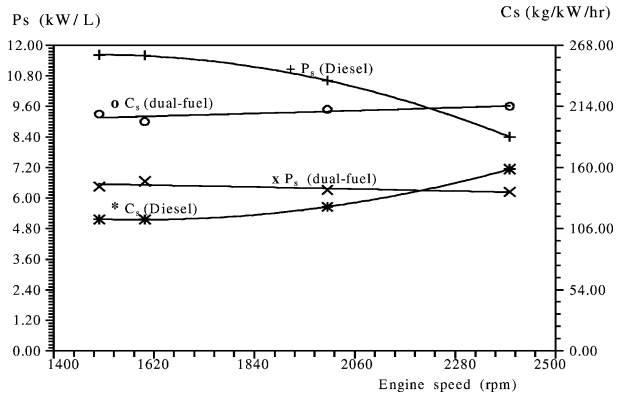

Figure 3. Brake specific fuel consumption and brake specific power as a function of engine speed for full load.

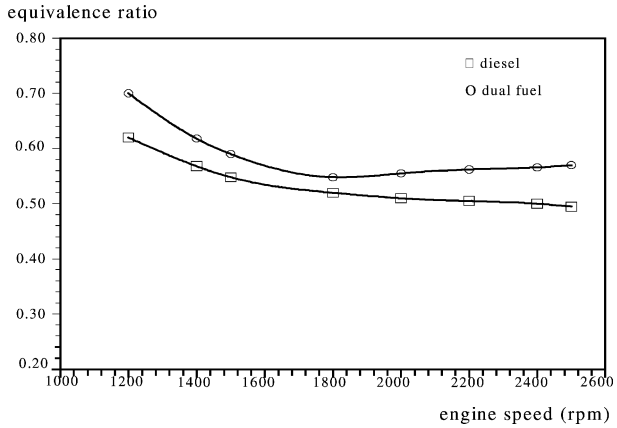

Figure 4. Fuel–air equivalence ratio versus engine speed for full load.

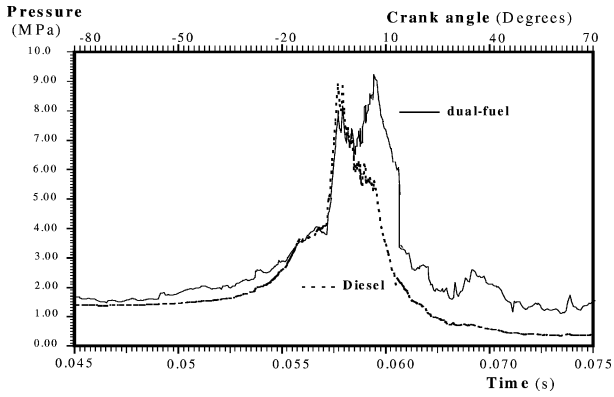

Figure 5. Cylinder pressure data for diesel and dual-fuel gas fueling for full loads at 1 000 rpm engine speed.

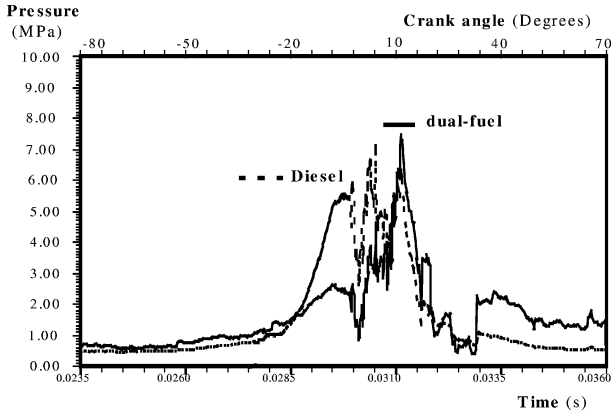

Figure 6. Cylinder pressure data for diesel and dual-fuel gas fueling for full loads at 2 000 rpm engine speed.

and natural gas. *Figure 4* shows the equivalence ratio, which is defined as the stoichiometric air-to-fuel mass ratio, divided by the measured air-to-fuel ratio, versus engine speed for full load for both diesel and natural gas fueling. As shown, the natural gas fueling compared to diesel fueling leads to slightly higher (less lean) equivalence ratios for a given speed condition. This occurs for two reasons. First, the natural gas is aspirated into the engine where it mixes with air, thereby displacing some portion of air, which could have moved into the cylinder. As less air is induced, the equivalence ratio increases. Secondly, as load is decreased, the engine is less efficient using natural gas hence more natural gas must be added to produce the fixed load-speed condition. The increased fueling then increases the equivalence ratio of the engine.

The cylinder gas pressure was measured using a piezoelectric transducer inserted into water cooled adapter and mounted in the main combustion chamber. It is connected to a digital acquisition system (DAS 1401). An incremental shaft encoder was coupled to the engine crankshaft to trigger the pressure data collection at one-half crank angle increments. *Figures 5* and *6* show the cylinder pressure data for diesel and dual fuel gas fueling for full loads at 1 000 and 2 000 rpm engine speed. Figures constructed with all recorded data were difficult to read due to overlapping. Therefore, graphical representation of the test data is given in the form of best-fit curves. The cylinder pressure data measured with natural gas fueling showed (*figures 5* and *6*) the second pressure peak occurring between 7 and 15 crank angles (depending on engine load and speed) after the corresponding pressure peak for diesel fueling. The double hump showed on the pressure trace, can be explained as the combustion of the pilot diesel charge followed by the natural gas combustion. The maximum combustion pressure for natural gas fueling is slightly higher for all engine speeds than the diesel fueling level. The general trend is governed by de-

creasing pressure and temperature levels with increasing speeds.

4. EMPIRICAL GAS–DIESEL (DUAL-FUEL) COMBUSTION MODEL

The empirical Gas–Diesel engine simulation has been carried out using the Wiebe model [26, 27] for different speeds and air–fuel ratios, in order to determine the influence of each one of the two parameters on the maximum temperature in the cylinder during the combustion cycle. The temperature has a great effect on the NO_x concentration [11, 12, 15, 28]. The dilution air ratio is obtained from an experimental investigation in the inlet and outlet manifold of the diesel engine converted to dual-fuel mode. The temperature variation is taken from the discretized equations of the temperature. From the first law of thermodynamics [26], extended to a steady flow (per step) case:

$$\frac{\mathrm{d}mu}{\mathrm{d}t} = -p\frac{\mathrm{d}V}{\mathrm{d}t} + \frac{\mathrm{d}Q}{\mathrm{d}t} + \sum h_i \frac{\mathrm{d}m_i}{\mathrm{d}t} \quad (1)$$

$$m\frac{\mathrm{d}u}{\mathrm{d}t} + u\frac{\mathrm{d}m}{\mathrm{d}t} = \frac{\mathrm{d}Q}{\mathrm{d}t} - p\frac{\mathrm{d}V}{\mathrm{d}t} + \sum_i h_i \frac{\mathrm{d}m_i}{\mathrm{d}t} \quad (2)$$

The specific internal energy (u) is function of the temperature (T) and composition (specified by the equivalence ratio F) of the gas, and is evaluated by using the thermochemical database of Chemkin (the chemical kinetics software from Sandia National Laboratories in USA [18]). Dissociation (pressure effect on a gas properties) is small and can be neglected. Thus, $u = u(T, F)$, hence:

$$\frac{\mathrm{d}u}{\mathrm{d}t} = \left(\frac{\partial u}{\partial T}\right)_F \frac{\mathrm{d}T}{\mathrm{d}t} + \left(\frac{\partial u}{\partial F}\right)_T \frac{\mathrm{d}F}{\mathrm{d}t} \quad (3)$$

The gas is assumed to be a perfect gas.

In addition, the heat transfer term ($\mathrm{d}Q/\mathrm{d}t$) can be divided into two components:

(1) The convective heat transfer from gas to cylinder wall $(\mathrm{d}Q/\mathrm{d}t)_{\mathrm{cv}}$, the convective heat transfer coefficient in the cylinder is calculated from Woshni and Hohenberg laws [31], and the change in wall temperature with time is given by a predictor-corrector routine.

(2) The energy released by the fuel combustion, during combustion in the cylinder only. The energy content of the fuel is specified by its specific enthalpy of formation (h_{for}) from its constituent elements at datum identical to that of the property subroutine.

Thus, the energy change due to the combustion of the fuel and heat transfer through the cylinder walls combine to give:

$$\frac{\mathrm{d}Q}{\mathrm{d}t} = \left(\frac{\mathrm{d}Q}{\mathrm{d}t}\right)_{\mathrm{cv}} + \frac{\mathrm{d}m_{\mathrm{c}}}{\mathrm{d}t} h_{\mathrm{for}} \quad (4)$$

Substituting equations (3) and (4) into energy equation (2), gives:

$$m\frac{\partial u}{\partial T}\frac{\mathrm{d}T}{\mathrm{d}t} + m\frac{\partial u}{\partial F}\frac{\mathrm{d}F}{\mathrm{d}t} + u\frac{\mathrm{d}m}{\mathrm{d}t} = \left(\frac{\mathrm{d}Q}{\mathrm{d}t}\right)_{\mathrm{cv}} + \frac{\mathrm{d}m_{\mathrm{c}}}{\mathrm{d}t} h_{\mathrm{for}} - \frac{mrT}{V}\frac{\mathrm{d}V}{\mathrm{d}t} + \sum_i h_i \frac{\mathrm{d}m_i}{\mathrm{d}t}$$

It is convenient separate the energy inflows and outflows, and express the equation in terms of $\mathrm{d}T/\mathrm{d}t$:

$$\frac{\mathrm{d}T}{\mathrm{d}t} = \left\{\left[\left(\frac{\mathrm{d}Q}{\mathrm{d}t}\right)_{\mathrm{cv}} + \frac{\mathrm{d}m_{\mathrm{c}}}{\mathrm{d}t} h_{\mathrm{for}} + \sum_i h_i \frac{\mathrm{d}m_i}{\mathrm{d}t}\right]\frac{1}{m} - \frac{rT}{V}\frac{\mathrm{d}V}{\mathrm{d}t} - \frac{\partial u}{\partial F}\frac{\mathrm{d}F}{\mathrm{d}t}\right\} \Big/ \frac{\partial u}{\partial T} \quad (5)$$

The cylinder temperature at the end of the step (T_2) is calculated from the initial value (T_1) and the weighted means of $\mathrm{d}T/\mathrm{d}t$, calculated using Adams–Bashford technique, from the current and the three previous steps. The time step (Δt) is correlated with the crank angle step ($\Delta\varphi$) of the engine by $\Delta t = \Delta\varphi/6N$.

Energy release schedules based on measured cylinder pressure as a function of crank angle were calculated using a one-zone thermodynamic analysis of the trapped cylinder diesel fuel–natural gas mixture. The analysis assumes uniform time varying thermodynamic properties in the engine and the energy release rate is calculated according the first law of thermodynamics for a single combustion zone as proposed by Heywood [26]. The diesel fuel burning rate is non-dimensionalised over the total mass of fuel delivered from the fuel pump per engine cycle per cylinder. A non-dimensional time is also introduced by defining an arbitrary total combustion duration of ($\Delta\varphi_T$) crank angle degrees from ignition to the end of burning. Actual crank angle is converted to non-dimensional time (φ^*) by:

$$\varphi^* = \frac{\varphi - \varphi_0}{\Delta\varphi_T} \quad (6)$$

The Wiebe model has been used for the fuel burning rate, as:

$$\frac{\mathrm{d}X_{\mathrm{b}}}{\mathrm{d}\varphi} = \frac{1}{\Delta\varphi_T} A B {\varphi^*}^{B-1} \mathrm{e}^{-A\varphi^{*B}} \quad (7)$$

TABLE V
The constants of the Wiebe model for natural gas combustion.

	$N \leq 1500$ rpm low BMEP ≤ 6.6	$N \leq 1500$ rpm medium BMEP	$N \leq 1500$ rpm high BMEP ≥ 12	$N \geq 1500$ rpm low BMEP ≤ 6.6	$N \geq 1500$ rpm medium BMEP	$N \geq 1500$ rpm high BMEP ≥ 12
A	3.82	5.05	6.67	3.95	4.67	5.52
B	1.87	1.412	1.07	2.06	2.67	3.45
Δt_T (ms)	9.33	6.65	4.75	3.22	2.81	2.46

Δt_T: global combustion time $\Delta t_T = \Delta\varphi_T/6N$.

The ignition point and ignition delay for diesel fuel are calculated from the dynamic injection point prediction (data) and an empirical correlation for ignition delay. Full details of the Wiebe model for natural gas combustion and the constants model used in this report have been estimated from the experimental study of the Diesel engine converted to spark ignition operation fueled with natural gas investigated previously [27]. Three combustion correlation options are available (*table V*). They can be selected by specifying the value of the brake mean effective pressure (BMEP) for low, medium and high BMEP. The ignition delay was defined as the time at which [O] × [CO] is maximum. Its value for the diesel fuel-natural gas mixture was computed by the sensitivity kinetics analysis (SENKIN) Chemkins' code [29, 30] for the engine conditions. A first estimate of ignition delay of the diesel fuel is modeled with Ahmed correlation [27]:

$$\tau = 9.426\left[\frac{N}{1000}\right]^{-0.94}\left[\frac{T_a}{300}\right]^{-2.89} P_c^{-0.482}\exp\left(\frac{877.5}{T_c}\right) \tag{8}$$

where T_c and P_c are respectively the mean gas temperature and the pressure during the engine compression phase.

5. GAS–DIESEL REACTION MECHANISM

Numerical modeling has become an essential part of combustion research for a better prediction of performances and emissions of many combustion systems. In combustion models, the importance of chemical kinetics has increased continuously. It has been proved, in fact, that a good representation of chemistry interactions is essential for predictive capabilities of numerical models. Moreover, the validity domain of a given model and its chemical kinetic sub-model in terms of temperature, pressure and equivalence ratio has to be large enough in order to include the wide range of operating conditions of many combustion systems. This is particularly true for the simultaneous prediction of carbon monoxide and unburned hydrocarbons, which are intermediate products of combustion in engines mainly formed at low ratings, and of nitrogen oxides, which are mostly produced at high temperature. Numerous studies in the field of chemical kinetics have been done in the past, leading to the conception of reaction mechanisms with growing complexity to describe the oxidation of a great variety of fuels. However, the models used for the combustion are restricted to single-step empirical expressions or global multistep schemes [17, 18]. The validity of such a quasi-global mechanism cannot be extended to the whole range of operating conditions of an engine, particularly at high pressure. The reaction mechanism of the oxidation of the natural gas used in the present work has been partially published previously [21–24]. It consists of 493 reactions among 81 species. The combustion under diesel engine conditions was modeled using the modified computer codes PSR (Perfect Stirred Reactor) developed at Sandia to by Kee and co-workers [19]. The transport properties and thermochemical quantities from the Sandia data were also used [20]. We have used the Burcat thermochemical data [32] for the compounds not found in the chemkin data base. The elementary reaction of the mechanism is written using the following formula:

$$\sum_{i=1}^{n}\alpha_{ij}X_i = \sum_{i=1}^{n}\beta_{ij}X_i \tag{9}$$

where α_{ij} and β_{ij} are the stoichiometric coefficient of species i in reaction j, for the reactants and products, respectively. The species conservation equation is given by [27]

$$\rho V\frac{dY_k}{dt} = -\dot{m}\left(Y_k - Y_k^*\right) + \dot{\omega}_k W_k V \tag{10}$$

The mass density ρ is calculated from the ideal gas equation of state: $\rho = P\overline{W}/(RT)$ where $\overline{W}$ is the mixture's mean molecular weight and (*) indicates the inlet conditions.

The energy equation in terms of temperature rather than enthalpy is stated as

$$Cp\frac{\mathrm{d}T}{\mathrm{d}t} = \frac{\dot{m}}{\rho V}\sum_{k=1}^{K} Y_k^*(h_k^* - h_k) - \sum_{k=1}^{K}\frac{h_k\dot{\omega}_k W_k}{\rho} - \frac{1}{\rho V}\left(\frac{\mathrm{d}Q}{\mathrm{d}t} - p\frac{\mathrm{d}V}{\mathrm{d}t}\right) \tag{11}$$

It is often interesting to determine how each reaction contributes to the production or destruction of species, the molar production of species is given by

$$\dot{\omega}_k = \sum_{i=1}^{I} \nu_{ki} q_i \tag{12}$$

where ν_{ki} are the stoichiometric coefficients and q_i are the rate of progress variables for the i reactions. The contribution to the rate production of species k for reaction i is therefore simply $C_{ki} = \nu_{ki} q_i$. These rates are computed from kinetic scheme and the rate constants of the elementary reactions using the modified Arrhenius equation:

$$k = AT^b \exp\left(-\frac{E}{RT}\right) \tag{13}$$

The normalized production and destruction values are given respectively by

$$\overline{C}_{ki}^{\mathrm{p}} = \frac{\max(\nu_{ki}, 0) q_i}{\sum_{i=1}^{I} \max(\nu_{ki}, 0) q_i} \tag{14a}$$

$$\overline{C}_{ki}^{\mathrm{d}} = \frac{\min(\nu_{ki}, 0) q_i}{\sum_{i=1}^{I} \min(\nu_{ki}, 0) q_i} \tag{14b}$$

Thus both sums: $\sum_{i=1}^{I} \overline{C}_{ki}^{\mathrm{p}} = 1$ and $\sum_{i=1}^{I} \overline{C}_{ki}^{\mathrm{d}} = 1$.

A detailed kinetic mechanism can be used to describe the oxidation of natural gas, but such detailed mechanisms are not known for higher hydrocarbons.

A description of the fuel kinetics is important, not only for predicting the amount of unburned fuel, but also to predict the species concentrations which participate in both the combustion and the pollutant species reactions. Although the carbon monoxide and nitric oxide kinetics are fairly well understood. When a detailed mechanism of fuel combustion kinetics is not available, some approximation are required to obtain estimates of these concentrations for calculating carbon monoxide and nitrogen oxide emissions. The reaction that represents the diesel fuel (DF) $C_{15}H_{32}$ was taken from the quasi-global model of Hautmann et al. [25], given as follows:

1. $C_nH_{2n+2} = (n/2)\,C_2H_4 + H_2$
2. $C_2H_4 + O_2 = 2\,CO + 2\,H_2$
3. $CO + \frac{1}{2}\,O_2 = CO$
4. $H_2 + \frac{1}{2}\,O_2 = H_2O$

This approach, termed quasi-global model, has been applied with some success to model energy-release rates for combustion of several hydrocarbon fuels [25, 33].

Nitric oxide and nitrogen dioxide are the major oxide of nitrogen emitted from combustion process. The sum of these species is reported as NO_x. In combustion, nitric oxide is the major component and NO_2 is formed from NO. Consequently models of NO_x kinetics focus on the formation of NO; this is sufficient except in cases where the NO/NO_2 ratio is required. Nitric oxide can be formed in the following way:

- from reactions of N_2 with oxygen "*thermal NO*";
- from nitrogen containing fuel compounds "*fuel NO*";
- from reactions of fuel-derived radicals with N_2 which ultimately lead to NO "*prompt NO*".

Thermal NO is formed via the extended Zeldovich mechanism [34, 35]. The steps in this mechanism may play an important role in all three paths to NO. The kinetics of thermal nitrogen fixation are well established [34, 35, 37, 38, 41, 42, 47, 50, 53]. Difficulties and approximations associated with use of these kinetics lies in the coupling of the NO reactions to the detailed kinetics schemes for hydrocarbon combustion. Models of nitric oxide formation from *fuel nitrogen* are limited due to the complexity of chemical steps through which the chemically-bound nitrogen passes. Because this nitrogen is bonded to the other fuel elements, a model for the reactions of this nitrogen will be just one portion of a detailed fuel combustion model [36–39]. A tentative mechanism, with estimated rate constants was proposed in several recent investigations [38, 40–44, 50, 51, 53, 55], the detailed models of prompt NO kinetics have not been established as yet. Because the amounts of prompt NO are small compared to other sources of NO [41, 42, 51] and prompt NO seems to occur mainly in rich flames [36, 44, 46]. There has been little interest in modeling the kinetics of prompt NO. Further quantities of prompt NO can be formed, due to radical overshoot, CN reactions or temperature fluctuations [41, 47]. Fenimore [40, 44] suggested that prompt NO might be due to reaction of fuel fragments with N_2 such as reactions 67–70 (*table VI*). The detailed chemistry calculation used in this study is an updated version developed from the original model by Kilpinen et al. [42]. The complete mechanism consists of 79 reactions given in *table VI*, and is specified and handled via chemical-kinetics

TABLE VI
Detailed chemical kinetic reaction mechanism of oxides of nitrogen (NO_x).

Reactions	A	b	E	Reactions	A	b	E
1. $N_2H_2+M=NNH+H+M$	5.00E+16	0.0	50 000.0	41. $N_2O+O=N_2+O_2$	1.00E+14	0.0	28 200.0
2. $N_2H_2+H=NNH+H_2$	5.00E+13	0.0	1 000.0	42. $HCN+O=CN+OH$	1.38E+06	2.1	6 121.0
3. $NNH+M=N_2+H+M$	2.00E+14	0.0	20 000.0	43. $HCN+O=NCO+H$	1.40E+04	2.6	4 980.0
4. $NNH+H=N_2+H_2$	3.70E+13	0.0	3 000.0	44. $HCN+O=NH+CO$	3.50E+03	2.6	4 980.0
5. $NNH+NO=N_2+HNO$	5.00E+13	0.0	0.0	45. $HCN+OH=CN+H_2O$	1.50E+13	0.0	10 929.0
6. $NH_3+M=NH_2+H+M$	1.40E+16	0.0	90 600.0	46. $HCN+OH=HOCN+H$	9.20E+12	0.0	15 000.0
7. $NH_3+H=NH_2+H_2$	7.00E+06	2.4	10 171.0	47. $HCN+OH=HNCO+H$	4.80E+11	0.0	11 000.0
8. $NH_3+O=NH_2+OH$	2.10E+13	0.0	9 000.0	48. $HCN+CN=C_2N_2+H$	2.00E+13	0.0	0.0
9. $NH_3+OH=NH_2+H_2O$	2.04E+06	2.0	566.0	49. $CN+O=CO+N$	1.02E+13	0.0	0.0
10. $NH_2+H=NH+H_2$	6.02E+12	0.0	0.0	50. $CN+OH=NCO+H$	5.00E+13	0.0	0.0
11. $NH_2+O=NH+OH$	6.90E+11	0.4	−201.0	51. $CN+H_2=HCN+H$	1.81E+14	0.0	7 962.0
12. $NH_2+O=HNO+H$	8.94E+14	−0.5	326.0	52. $CN+O_2=NCO+O$	5.60E+12	0.0	0.0
13. $NH_2+OH=NH+H_2O$	4.33E+05	1.7	0.0	53. $CN+NO_2=NCO+NO$	3.00E+13	0.0	0.0
14. $NH_2+N=N_2+H+H$	7.20E+13	0.0	0.0	54. $CN+N_2O=NCO+N_2$	1.00E+13	0.0	0.0
15. $NH_2+NH=N_2H_2+H$	5.00E+13	0.0	0.0	55. $NCO+M=N+CO+M$	3.10E+16	−0.5	48 000.0
16. $NH_2+NO=NNH+OH$	8.80E+15	−1.3	0.0	56. $NCO+H=NH+CO$	5.00E+13	0.0	0.0
17. $NH_2+NO=N_2+H_2O$	3.80E+15	−1.3	0.0	57. $NCO+O=NO+CO$	4.21E+13	0.0	0.0
18. $NH+H=N+H_2$	3.00E+13	0.0	0.0	58. $NCO+OH=NO+CO+H$	1.00E+13	0.0	0.0
19. $NH+O=NO+H$	2.00E+13	0.0	0.0	59. $NCO+H_2=HNCO+H$	8.60E+12	0.0	9 000.0
20. $NH+OH=HNO+H$	2.00E+13	0.0	0.0	60. $NCO+N=N_2+CO$	2.00E+13	0.0	0.0
21. $NH+OH=N+H_2O$	5.00E+11	0.5	2 000.0	61. $NCO+NO=N_2O+CO$	1.00E+13	0.0	−390.0
22. $NH+O_2=HNO+O$	1.00E+13	0.0	12 000.0	62. $HOCN+H=HNCO+H$	1.00E+13	0.0	0.0
23. $NH+O_2=NO+OH$	1.40E+11	0.0	2 000.0	63. $HCNO+H\Rightarrow HCN+OH$	5.00E+13	0.0	12 000.0
24. $NH+NO=N_2O+H$	8.00E+13	0.0	14 800.0	64. $HNCO+H=NH_2+CO$	2.00E+13	0.0	3 000.0
25. $NH+N=N_2+H$	3.00E+13	0.0	0.0	65. $C_2N_2+O=NCO+CN$	4.60E+12	0.0	8 880.0
26. $N+O_2=NO+O$	6.40E+09	1.0	6 280.0	66. $C_2N_2+OH=HOCN+CN$	1.90E+11	0.0	2 900.0
27. $N+OH=NO+H$	3.21E+13	−0.3	0.0	67. $C+NO=CN+O$	1.00E+14	0.0	0.0
28. $N+NO=N_2+O$	3.30E+12	0.3	0.0	68. $C+N_2O=CN+NO$	1.00E+13	0.0	0.0
39. $NO+HO_2=NO_2+OH$	1.90E+11	0.0	3 400.0	69. $CH+NO=HCN+O$	1.10E+14	0.0	0.0
30. $NO_2+M=NO+O+M$	5.00E+13	0.0	0.0	70. $CH+N_2=HCN+N$	2.50E+11	0.0	13 600.0
31. $NO_2+H=NO+OH$	2.10E+12	0.0	−480.0	71. $CH+NH_2=HCN+H+H$	3.00E+13	0.0	0.0
32. $NO_2+O=NO+O_2$	1.10E+16	0.0	66 000.0	72. $CH+NH=HCN+H$	5.00E+13	0.0	0.0
33. $HNO+M=H+NO+M$	3.50E+14	0.0	1 500.0	73. $CH+N=CN+H$	1.30E+13	0.0	0.0
34. $HNO+H=H_2+NO$	1.00E+13	0.0	600.0	74. $CH_2+NO\Rightarrow HCNO+H$	1.40E+12	0.0	−1 100.0
35. $HNO+OH=NO+H_2O$	1.50E+16	0.0	48 680.0	75. $CH_2+N_2=HCN+NH$	1.00E+13	0.0	74 000.0
36. $N_2O+M=N_2+O+M$	5.00E+12	0.0	0.0	76. $CH_2+NH=HCN+H+H$	3.00E+13	0.0	0.0
37. $N_2O+H=N_2+OH$	3.60E+13	0.0	0.0	77. $CH_2+N=HCN+H$	5.00E+13	0.0	0.0
38. $N_2O+O=NO+NO$	1.60E+14	0.0	51 600.0	78. $CH_3+N=HCN+H+H$	5.00E+13	0.0	0.0
39. $N+CO_2=NO+CO$	7.60E+13	0.0	15 200.0	79. $CH_4+N=NH+CH_3$	1.00E+13	0.0	24 000.0
40. $N+HCCO=HCN+CO$	1.00E+14	0.0	28 200.0				

package Chemkin [24]. The NO_x formation mechanism may be summarized schematically by *figure 7*. The principal nitrogen-containing pollutants emitted by combustion devices are NO and NO_2. However, in discussion of the chemistry of nitrogen oxides [49–53, 56], it is noticed that nitrogen-containing compound (e.g., HCN, CN, NH_i, lower amine RNH_2, and various nitrates and nitrites and nitro-olefins) were formed during combustion of hydrocarbon fuels. The kinetic scheme requires some approximations because the detailed mechanism for reactions of species such as NH, NH_2, CN, NCO, etc. is not fully known, and rate constants for most of the established reactions are estimates or taken from experimental values with large uncertainties. For the most part, the concentration of these species in the exhaust gas are small (< 1 ppm) [51, 52, 56]. Most of the data are taken from

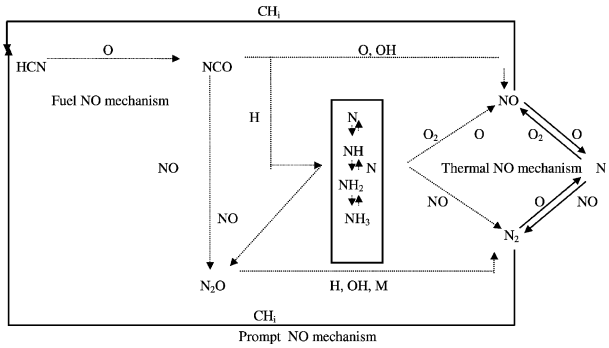

Figure 7. Summary of the principal NO_x formation and destruction kinetics [38].

Kilpinen et al. [42], Clarborg et al. [51], Kristensen et al. [53] and Alzueta et al. [55]. The reaction rate of k_k for kth reaction is given by $k_k = AT^b \exp(-E/RT)$, with the activation energy E in cal·mol^{-1} and R is the universal gas constant and the pre-exponential factor A in mol-cm-s-K. NO formed during combustion can subsequently react with nitrogen-containing intermediates to form N_2, NO also may react with various oxygen-containing species to form NO_2. Nitrogen dioxide concentrations are generally negligibly small compared to NO concentrations [45, 50, 52, 53]. Relatively large concentration of NO_2 can be formed in the combustion zone inside the engine cylinder, followed by subsequent conversion of the NO_2 back to NO in the post-flame region (in burnout process). NO_2 is thus generally considered to be a transient intermediate species, which only exists at flame conditions [49, 50, 52, 54, 55]. Rapid mixing of hot and cold regions of the turbulent reacting flows can result in a rapid quenching of the NO_2, followed by subsequent emission in the exhaust gases [44, 46, 47].

6. SEQUENCE OF THE SIMULATION ALGORITHM

"Divide and conquer" is an often-used strategy to tackle complex problems. In its application to the current one, the division is between main heat-releasing and species-producing reactions and the pollutant formation and destruction kinetics. In essence, the technique consists in calculating the energy release rate and temperature is based on measured cylinder pressure as a function of crank angle according the first law of thermodynamics for a single combustion zone. Then, the chemical system is integrated over the time using the cylinder composition and temperature. A stiff-system solver (namely, the well-known LSODE routine [29, 30]) is used for this integration. At the end of time-step, a new composition, temperature and pressure are obtained. The method is of course CPU-time intensive, but it makes the task just manageable. The numerical model calculates in discrete crank angle incremental steps from bottom dead center (BDC) at the start of the compression stroke, through compression, combustion and expansion to BDC, and at the end of expansion stroke. Variation of valve timing, from BDC and TDC (top dead center) are not directly considered, other than by calculating the volume of fresh air-natural gas entering the cylinder from experimental data that is valve timing dependent. Conditions in the cylinder are assumed to be known, the homogeneous mixture of air and combustion products (of varying composition), behaving as a perfect gas. Calculations for a specified crank angle step consist of applying the energy equation (from the first law of thermodynamics), hence relating the heat transfer rate to the work transfer rate (the piston work) to the change of internal energy of the gas mixture. Heat transfer to or from the gas is also calculated. Combustion, when appropriate, is calculated from the rate at which the fuel is burned (from Wiebe model). This calculates the rate of fuel burning by combustion as a function of engine speed, and the equivalence ratio (F) calculated from the total mass of fuel and air in the cylinder. This is linked to energy transfer by formation enthalpy of the fuel mixture. During the combustion phase, the temperature calculated using the Wiebe model, is used for solving the temperature-fixed problem by the PSR code, whose solutions serve as the first iterate for the solution of the full problem including the coupled energy-species equation. The normalized rate of destruction values $\overline{C}_{ki}^{\mathrm{d}}$ for species destruction are determined for hydrocarbon species (*figure 12*). The new Wiebe model constants are computed from $\overline{C}_{ki}^{\mathrm{d}}$ values (equation (14b)). The work transfer rate (work done by the piston) is calculated by integrating the cylinder pressure and the change in cylinder volume during the step (this is assumed for each step to calculate total work done per engine cycle and hence torque output). The change of cylinder volume with crank angle is calculated from the piston crank geometry. In-cylinder mixture mass is calculated from conservation of mass. This is constant except during combustion, when diesel fuel is considered to be added at a rate equal to the fuel burning rate. A predictor–corrector routine is used to iterate until converged solution per step is obtained.

7. SIMULATION RESULTS

The computation program was used in conjunction with the experimental data and provided a means for fur-

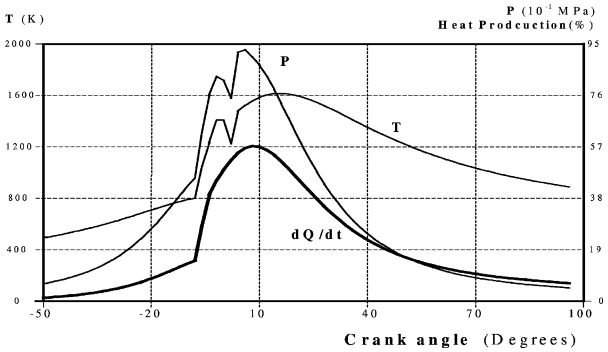

Figure 8. Predicted cylinder pressure, temperature and rate of heat production evolution results for 1 000 rpm engine speed and 0.7 fuel–air equivalence ratio at full load.

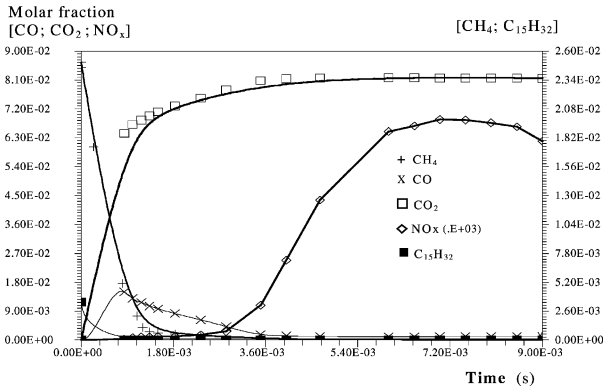

Figure 9. Predicted molecular species profiles obtained for dual-fuel mode operation for 1 000 rpm engine speed and 0.7 fuel–air equivalence ratio at full load.

ther investigation of trends established through experiments. A computational study has been undertaken and the results presented are plausible, showing reasonable agreement with some experimental engine data. It is clear that the diesel fuel burns first, providing the energy required to ignite the lean gas mixture (natural gas–air). *Figures 8–11* show the results of the dual-fuel combustion simulation with natural gas as fuel. *Figures 8* and *10* represent the pressure, the temperature and the heat production rate evolution in the cylinder during the (compression, combustion and expansion) phases of the cycle for two engine speeds 1 000 and 2 000 rpm for a static advance with respect to the injection system of 28 crank angle degrees bTDC (before top dead center). One notices that a displacement of the maximal peaks sizes after TDC (top dead center) occurs with the increase of the engine speed, in spite of the centrifugal correction of the injection system for the dynamic advance, which is related to the engine speed. These results are qualitatively consistent with the experimental engine results presented

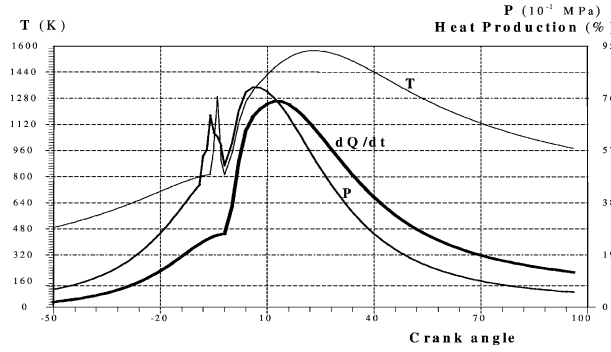

Figure 10. Predicted cylinder pressure, temperature and rate of heat production results for 2 000 rpm engine speed and 0.58 fuel–air equivalence ratio at full load.

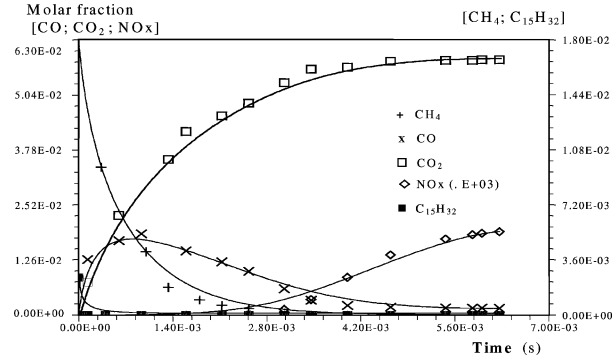

Figure 11. Predicted molecular species profiles obtained for dual-fuel mode operation for 2 000 rpm engine speed and 0.58 fuel–air equivalence ratio at full load.

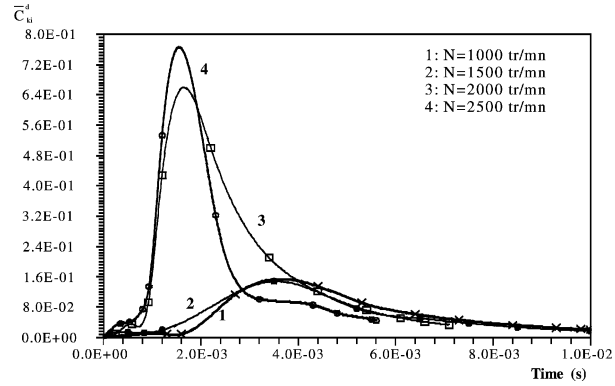

Figure 12. The computed profiles of normalized rate of destruction values $\overline{C}_{ki}^{d}$ for hydrocarbon species with engine speed at full load for dual-fuel mode.

in *figures 5* and *6*. This remark is due essentially to the induction time of the auto-ignition reaction of the fuel in a very lean mixture.

Experimental pressure data (*figures 5* and *6*) shows similar dual pressure peak traces. Computed results predict with reasonable accuracy the main combustion characteristics (pressure and concentrations species) under the all conditions of this study. The controlling steps of the dual-fuel combustion are then identified using computational results. Good prediction is observed in *figures 5–8* and *figures 6–10* for cylinder pressure data. For nearly all cases, reasonably unbiased errors are located within [−5 %, +5 %] for pressure. *Figures 8–10* show the temperature and heat release rates, as calculated from PSR code, versus crank angle. Overall, the two parameters can be described as having dual peaks (much less pronounced for the heat release rate), a characteristic that is similar to measured and predicted pressure. The early peak occurs as a result of the rapid combustion of the diesel fuel during the natural gas ignition delay period. The second energy release period occurs as a result of natural gas combustion. The dual peak characteristic has been reported in some studies by Kakwani et al. [57] and Hsu [58]. The range of pressure and temperature experienced by the reactants (mixture fuel–natural gas–air) drawn into the cylinder is particularly wide, hence a very extensive variety of chemical reactions taking place.

The characteristic chemical time of natural gas oxidation, has been defined from the computed concentration profiles as the time delay of the trapped cylinder gas after auto-ignition fuel period as estimated by Fraser et al. [13]. Concentration profiles of major products (carbon monoxide, carbon dioxide, methane, oxides of nitrogen and diesel fuel) are deduced from a simulation work taking into account two-time step detailed kinetic model. At high engine speed, during the first stage of the reaction when the fuel and oxygen are consumed at a wide rate, C_2H_4 and C_2H_6 are formed in appreciable amount (the fuel auto-ignition period is less than 0.5 ms). The rank ordering of the reaction rates indicates that the most important path is the Hautmann reaction mechanism. At high temperature in engine speeds range less than 1500 rpm (the fuel auto-ignition delay is more than 0.75 ms as show in *figure 9*). Auto-ignition appears as a single-stage flame and the induction period decreases with pressure (*figure 9*).

The predicted NO mass fraction by the complete mechanism decreases as the engine speed in full load increases. This result can be attributed to the increase of the NO reactivity due to increase of reaction pressure and temperature with time (*figures 9* and *11*).

TABLE VII
The new computed constants of the Wiebe model for dual fuel combustion at full load condition.

N (rpm)	1 000	1 500	2 000	2 500
A	2.916	2.17	3.22	5.74
B	1.92	2.066	2.27	3.45
Δt_T (ms)	13.88	8.75	6.22	5.46

8. EMISSION RESULTS

Emissions of total hydrocarbons (C_mH_n), carbon monoxide (CO), carbon dioxide (CO_2), nitrogen oxides (NO_x) were measured at the engine exhaust. The sample stream was cooled and dried in a thermostatic sample conditioner before being analyzed by the flame ionization detection instruments (FID RS55 used for C_mH_n), non-dispersive infrared (NDIR Beryl used for CO and CO_2), and chemiluminescent (Topaze 2020 used for NO_x).

Figure 13 shows CO and NO_x emission concentrations measured in the exhaust gas as a function of engine speed for full load for diesel and natural gas fueling. CO emissions were increased for natural gas fueling. This is consistent with the fuel–air ratio results (*figure 4*) and explanations for non-optimized pilot timing, flame quenching and partial burning. It is expected that the elevated fuel–air ratio for natural gas fueling, would be accompanied by higher CO emissions. The chemical composition of NO_x used in the present study is the *Total Fixed Nitrogen* [41, 51, 53] and is stated as $TFN = [NO] + [NO_2] + 2[N_2O]$. The NO_x emissions are affected directly by the change of air–fuel ratio. The natural gas–air mixture leaning with increasing engine speed, which would induces a slower flame propagation [4]. NO_x concentrations were reduced at high speed (greater than about 1 500 rpm) for natural gas fueling. Due to the slow kinetics of NO_x formation, the residence

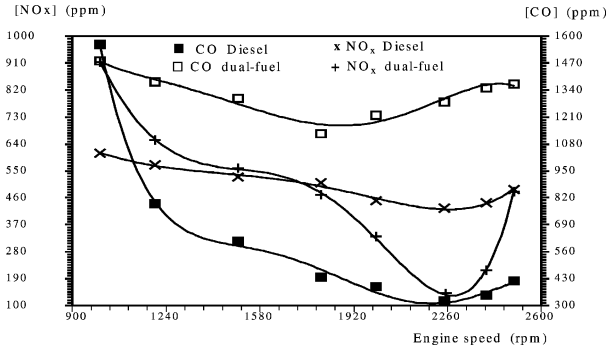

Figure 13. NO_x and CO emissions as a function of engine speed for full loads dual-fuel/diesel.

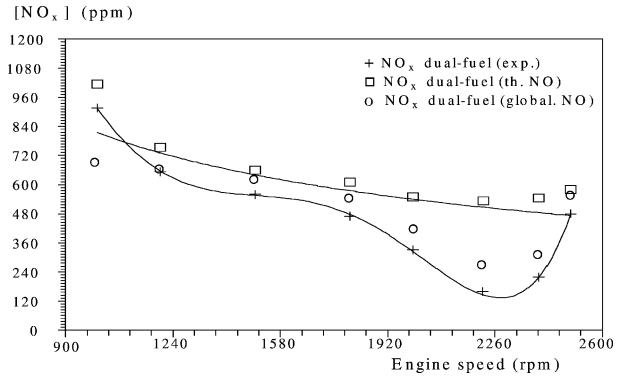

Figure 14. NO_x emissions as a function of speed for full loads dual-fuel (simulated results, □: thermal NO, ○: complete mechanism, +: experimental results).

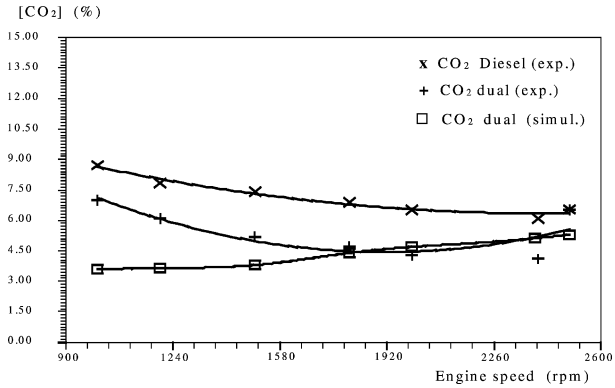

Figure 15. CO_2 emissions as a function of speed for full loads dual-fuel (×, +: experimental results, □: simulated results).

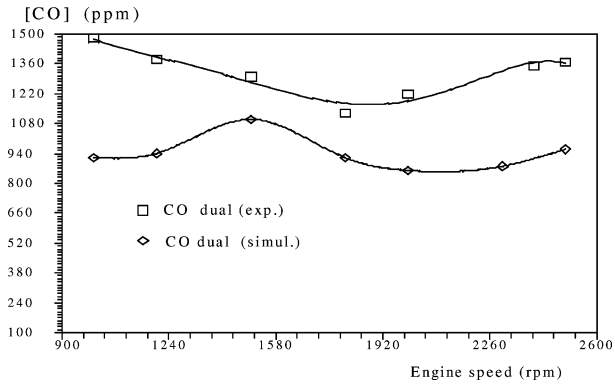

Figure 16. CO emissions as a function of engine speed for full load dual-fuel (experimental and simulated results).

time of gases inside the cylinder is one of the key parameters. As demonstrated by several papers [42, 43, 47–50, 54], the natural gas reburning technique has a higher reduction potential compared with other NO_x reduction techniques in lean mixture.

The NO_x emission characteristic of the gas engine is determined by the air–fuel ratio when the ignition timing is constant. It is widely known that the concentration of NO_x emission reaches a maximum in the vicinity of the air excess around 10 %, and decreases sharply in the range of high air–fuel ratio, that is so called the lean mixture (at the level of high air–fuel ratio combustion temperature drops and NO_x concentration lowers exponentially). The general trend is increasing air–fuel ratio with increasing engine speed for natural gas fueling. However, the problem with lean burn is cycle-to-cycle fluctuations in ignition and combustion. Combustion cycle fluctuations lead to torque and engine speed and reduction in combustion efficiency [12]. The minimum ignition energy of gas fuel is related to the air–fuel ratio. The higher air–fuel ratio is, the larger energy required for ignition. The ignition delay time increases at high air–fuel ratio, thus in real engine, the potential combustion period is limited by the engine speed and the combustion of fuel gas tends to be incomplete [8].

The quench area near the combustion chamber wall increases as air–fuel ratio goes higher. As a result, it is supposed that the thermal efficiency will go down and unburned HC and CO concentrations increase (*figure 13*). It is expected that elevated CO concentrations would be accompanied by higher unburned hydrocarbons (only the natural gas fueling measured concentration are presented graphically, *figure 17*). CO_2 emissions were decreased for natural gas fueling (*figure 15*). Ignition of lean natural gas mixtures is difficult to achieve and can result into incomplete combustion or total misfire. For ignition to be successful, the energy release rate in early stages of ignition must be greater than losses from ignition flame kernel. Otherwise, the flame extinguishes prematurely. For lean mixtures, the energy release per unit volume is less, because the fuel charge is diluted with excess air. *Figure 14* shows measured and computed concentration of NO_x as a function of engine speed for full load condition. The computed values are generally overpredicted by the Zeldovich mechanism. Nevertheless, we observed (*figure 14*) better agreement between experimental and computed concentration profiles by the global mechanism. NO_2 is generated as an intermediate species in the nitrogen chemistry within the reacting zone, but is destroyed in the burnout process. As the engine speed decreases, the reaction rates of the NO_2 destruction mechanisms are slower and a slightly higher residual concentration can be detected at the exit. Nevertheless, the exit concentrations are lower than 20 ppm in all tests.

Figure 16 shows measured and computed concentrations of CO as a function of engine speed for full load.

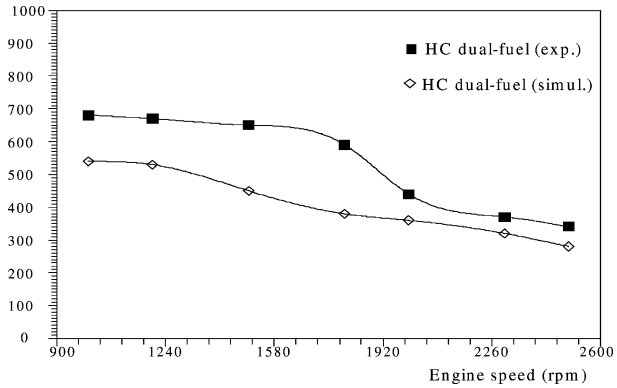

Figure 17. HC emissions as a function of engine speed for full load dual-fuel (experimental (■) and simulated (◇) results).

The computed values are lower than the measured ones by 10 % at 1 500 rpm engine speed to 30 % at 1 000 rpm. Predicted and measured HC emission concentrations in the exhaust gas as a function of engine speed for full load for natural gas fueling only, are shown in *figure 17*. The trend of the measured and simulated values are similar. The HC concentrations are decreased with increasing engine speed. The measured values being slightly higher (about 15 %) than computed values at engine speeds below 1 800 rpm.

9. CONCLUSION

The emission and performance characteristics of a commercial diesel engine (Deutz FL8 413F) operated on natural gas with pilot diesel ignition were investigated. A computer program has been developed to model the experimental data using a chemical kinetic reaction mechanism of the Gas–Diesel (dual-fuel) combustion. A detailed chemical kinetic reaction mechanisms of natural gas (NG) and NO_x were used to predict with reasonable accuracy the main combustion characteristics (temperature, pressure and species concentrations) under the conditions of this study. A kinetic analysis was performed in order to identify the controlling steps of the dual-fuel combustion. The credibility of this work depends on the ability of the numerical model to restitute the instantaneous fuel conversion rates under all the experimental engine conditions, not only for predicting the amount of unburned fuel, but also to predict the species concentrations that participate in both process the combustion and the pollutant reactions. The results of the comparison between computed and experimental results appear in *figures 14–17* where we can see that the experimental data are well reproduced by the chemical kinetic reaction mechanism of the natural gas–diesel fuel oxidation. The application of such kinetic models is reasonable when the object is the prediction of trends. Good agreement between a model and experiment cannot be considered as a verification of the validity of the approximate model. Instead, such good agreement between model and experiment should be regarded as a verification of the utility of the model for prediction under the same conditions as used in the experiment.

Acknowledgements

This research was supported by GNV-Project (SONATRACH L.T.G) which is gratefully acknowledged. We would like to thank Prof. M. Cathonnet (Directeur LCSR-CNRS-Orléans, France) for providing a copy of the natural gas mechanism and helpful comments on the manuscript. Furthermore, the editor and the referees are to be thanked for their constructive comments.

REFERENCES

[1] Hodgins K.B., Gunawan H., Hill P.G., Intensifier injector for natural gas fueling of diesel engines, SAE Paper 921553 (1992) 29–39.

[2] Karim G.A., The dual-fuel engine of compression ignition type-prospects, problems and solutions, in: SAE Technical Paper Series, Compressed Natural Gas as a Motor Vehicle, Pittsburgh, PA, 1983, pp. 312–321.

[3] Al-himyary T.J., Karim G.A., A correlation for the burning velocity of methane–air mixtures at high pressures and temperatures, J. Eng. Gas Turbine and Power 109 (1987) 439–451.

[4] Quader A.A., Lean combustion and the misfire limit in spark ignition engines, SAE Paper 741055 (1974) 590–601.

[5] Tesarek H., Investigation concerning the employment possibilities of the Diesel–Gas process for reducing exhaust emission especially soot (particulate matters), SAE Paper 750158 (1975) 445–458.

[6] Xianhua D., Hill P., Emissions and fuel economy of a prechamber diesel engine with natural gas dual-fueling, SAE Paper 860069 (1986) 1269–1282.

[7] Boisvert J., Gettel L.E., Perry G.C., Particulate emissions for a dual-fuel caterpillar 3208 engine, ASME Paper 88-ICE-18 (1988) 277–285.

[8] Martin J.K., Plee S.L., Remboski D.J., Burn modes and prior-cycle effects on cyclic variations in lean-burn spark-ignition engine combustion, SAE Paper 880201 (1988) 85–102.

[9] Mills F.D., Ultra lean burn exhaust emissions characteristics and control, ASME ICE 8 (1988) 480–487.

[10] Acker G., Brett C.E., Schaetzle W.J., Song Y.K., LNG (Liquid Natural Gas) as a fuel and refrigerant for diesel powered shrimp boats, ASME Paper 88-ICE-21 (1988) 63–72.

[11] Kingston Jones M.G., Heaton D.M., Nebura combustion system for lean burn spark ignited gas engines, SAE Paper 890211 (1989) 211–227.

[12] Saturo G., Yasuhiro I., Yutaka H., Tateo N., Niigata ultra lean burn SI gas engines — achieving high effficiency and low NO_x emission, SAE Paper 901608 (1990) 1933–1951.

[13] Fraser R.A., Siebers D.L., Edwards C.F., Autoignition of methane and natural gas in a simulated diesel environment, SAE Technical Paper 910227 (1991) 192–200.

[14] Edwards C.F., Siebers D.L., Hoskins D.H., A study of the autoignition process of a diesel spray via high speed visualization, SAE Technical Paper 920108 (1992) 23–62.

[15] Doughty G.E., Bell S.R., Midkiff K.C., Natural gas fueling of a caterpillar 3406 diesel engine, J. Eng. Gas Turbines Power 114 (1992) 459–465.

[16] Blizzard D.T., Schaub F.S., Smith J.G., Development of the Cooper–Bessemer Clean Burn^{TM} Gas–Diesel (dual-fuel) engine, J. Eng. Gas Turbines and Power 114 (1992) 480–487.

[17] Bounif A., Mansour C., Aris A., Some results on combustion of natural gas in diesel engine, in: Fifth Int. Conference on Technologies and Combustion for Clean Environment, Lisbon, Portugal, 1999, pp. 726–735.

[18] Mansour C., Bounif A., Aris A., Combustion modeling of natural gas in diesel engine: experiments and computations, in: Urban Transport 99, Wessex Institute of Technology, 8–10 September, Rhodes Greece, WIT Press, 1999, pp. 212–221.

[19] Kee R.J., Grcar J.F., Smooke M.D., Miller J.A., Sandia National Laboratories Report SAND 85–8240, 1985.

[20] Kee R.J., Dixon-Lewis G., Warnatz J., Coltrin M.E., Miller J.A., Sandia National Laboratories Report SAND 86–8246, 1986.

[21] Tan Y., Dagaut P., Cathonnet M., Boettner J.C., Combust. Sci. Tech. 96 (1994) 133–158.

[22] Tan Y., Dagaut P., Cathonnet M., Boettner J.C., Int. J. Chem. Kinet. 92 (1995) 726–739.

[23] Tan Y., Dagaut P., Cathonnet M., Boettner J.C., Backman J.S., Carlier P., in: 25th Symposium Int. on Combustion, The Combustion Institute, Pittsburgh, 1995, pp. 1563–1572.

[24] Dagaut P., Cathonnet M., Boettner J.C., Combust. Sci. Tech. 58 (1992) 867–884.

[25] Hautmann D.J., Dryer F.L., Schug K.P., Glassman I., Comb. Sci. Tech. 25 (1981) 219–235.

[26] Heywood J.B., Internal Combustion Engine Fundamentals, McGraw-Hill, New York, 1988.

[27] Harouadi F., Contribution à l'étude de la cinétique de la combustion en limite pauvre dans les moteurs alimentés en gaz naturel, Ph.D. thesis, The University of Aix Marseille, 1993.

[28] Ranzi E., Sogaro A., Gaffuri P., Pennati G., Faravelli T., Combust. Sci. Tech. 96 (1994) 279–325.

[29] Hindmarsh A.C., Byrne G.D., ACM Trans. Math. Software, 1–71.

[30] Wang H., Frenklach M., Combustion and Flame 34 (1975) 173–221.

[31] Woshni G., Universally applicable equation for the instantaneous heat transfer coefficient in the internal engines, SAE Paper 670931 (1967) 421–428.

[32] Burcat A., Thermochemical data for combustion and calculations, in: Gardiner W.C. Jr. (Ed.), Combustion Chemistry, Springer Verlag, New York, 1984.

[33] Edelman R., Economos C., A mathematical model for jet engine combustor pollutant emissions, AIAA 71 (1971) 714–726.

[34] Westenberg A.A., Combust. Sci. Technol. 4 (1971) 59–78.

[35] Zeldovich Y.B., The Mathematical Theory of Combustion and Explosions, Consultants Bureau, New Work, NY, 1985.

[36] Fenimore C.P., Combustion and Flame 19 (1972) 289–301.

[37] De Soete G., Rev. Inst. Franc. de Petrole 28 (1973) 95–109.

[38] De Soete G., Overall reaction rate of NO and N_2 formation from fuel nitrogen, in: 15th Combustion Symposium, Tokyo, Japan, 1974, pp. 1011–1024.

[39] Flagan R.C., Galant S., Appleton J.P., Combustion and Flame 22 (1974) 299–315.

[40] Fenimore C.P., in: 13th Int. Symp. on Comb., The Combustion Institute, 1971, pp. 373–382.

[41] Norman A.C., Prog. Energy Combust. Sci. 1 (1975) 3–15.

[42] Kilpinen P., Glarborg P., Hupa M., Reburning chemistry: a kinetic modeling study, Ind. Eng. Chem. Res. 31 (1992) 1477–1490.

[43] Wendt J.O.L., Sterling C.V., Matovich M.A., Reduction of SO_3 and NO_x by secondary fuel injection, in: 14th Sym. Int. on Comb., 1972, pp. 897–910.

[44] Fenimore C.P., Formation of NO in premixed hydrocarbon flames, in: 13th Symp. Int. on Comb., 1973, pp. 373–382.

[45] Myerson A.L., Reduction of NO in simulated combustion effluents by hydrocarbon/O_2 mixtures, in: 15th Symp. Int. on Comb., 1974, pp. 1085–1094.

[46] Chen S.L., McCarthy J.M., Bench and pilot scale process evaluation of reburning for in-furnace NO_x reduction, in: 21st Symp. Int. on Comb., 1986, pp. 1159–1168.

[47] Lanier W.S., Mulholland J.A., Beard J.T., Reburning thermal and chemical processes in a two-dimensional pilot-scale system, in: 21st Symp. Int. on Comb., 1986, pp. 1171–1179.

[48] Mereb J.B., Wendt J.L., Reburning mechanisms in a pulverized coal combustor, in: 23rd Symp. Int. on Comb., 1990, pp. 1273–1279.

[49] Mereb J.B., Wendt J.L., Air staging and reburning mechanisms for NO_x abatement in a laboratory coal combustor, Fuel 73 (1994) 1020–1026.

[50] Bilbao R., Millera A., Alzueta M.U., Influence of the temperature and oxygen concentration on NO_x reduction in the natural gas reburning process, Ind. Eng. Chem. Res. 33 (1994) 2846–2852.

[51] Glarborg P., Miller J.A., Mechanism and modeling of HCN oxidation in a flow reactor, Combustion and Flame 99 (1994) 475–483.

[52] Nelson P.F., Haynes B.S., Hydrocarbon/NO_x interactions at low temperatures, conversion of NO to NO_2 by propane and the formation of HNCO, in: 25th Symp. Int. on Comb., 1994, pp. 1003–1010.

[53] Kristensen P.G., Glarborg P., Dam-Johansen K., Nitrogen chemistry during burnout in fuel-staged combustion, Combustion and Flame 107 (1996) 211–222.

[54] Rutar T., Kramlich J.C., Malte P.C., N_2O emissions control by reburning, Combustion and Flame 107 (1996) 453–463.

[55] Alzueta M.U., Glarborg P., Dam-Johansen K., Low temperature interactions between hydrocarbons and NO: an experimental study, Combustion and Flame 109 (1997) 25–36.

[56] Bilbao R., Alzuata M.U., Millera A., Prada L., Dilution and stoechiometry effects on gas reburning: an experimental study, Ind. Eng. Chem. Res. 36 (1997) 2440–2444.

[57] Kakwani R.M., Winsor R.E., Energy sources technology conference and exibitions, ASME ICE 16 (1990) 25–32.

[58] Hsu B.D., Preliminary full load test, ASME ICE 5 (1988) 39–46.

[59] Natural gas composition and properties and the fluctuation over the period of three years (1994–97), Sonatrach–LTG Laboratories Report LTG 97–108, 1997.